Light-scattering spectroscopy of the liquid-glass transition in $CaKNO_3$ and in the molecular glass Salol: Extended-mode-coupling-theory analysis

H. Z. Cummins and W. M. Du
City College of the City University of New York, New York, New York, 10031

M. Fuchs, W. Götze,* S. Hildebrand, and A. Latz†
Physik Department, Technische Universität München, D-8046 Garching, Germany

G. Li and N. J. Tao‡
City College of The City University of New York, New York, New York 10031

(Received 4 December 1992)

Recently reported light-scattering studies of $CaKNO_3$ and Salol are reanalyzed, using the extended version of the mode-coupling theory of the liquid-glass transition including activated transport or hopping effects. Problems found in the original fits due to the neglect of hopping terms are largely corrected, and quantitative predictions for the susceptibility minimum below the crossover temperature T_c are found. The results are also shown to accurately explain the $CaKNO_3$ neutron spin-echo data reported by Mezei [J. Non-Cryst. Solids **131–133**, 317 (1991)].

PACS number(s): 64.70.Pf, 78.35.+c, 61.20.Lc

I. INTRODUCTION

Investigations of the liquid-glass transition have traditionally concentrated on the region of the calorimetric glass-transition temperature T_g where the viscosity reaches 10^{13} P, the primary α-relaxation time increases to ~ 100 s or longer, and anomalies may occur in the specific heat [1,2]. Recently, however, attention has shifted to the range of supercooled-liquid temperatures extending upwards from T_g to the bulk melting temperature T_m. Interest in this region was stimulated by the appearance of a theoretical approach to the liquid-glass transition which analyzes the effects of nonlinear interaction between density-fluctuation modes self-consistently. Proposed in 1984 [3–5], the mode-coupling theory (MCT), in its original idealized form, predicts that as the strength of the nonlinear interactions increases with decreasing temperature, an ergodic to nonergodic transition will occur at a crossover temperature T_c with many of the properties of the experimental liquid-glass transition. A number of recent experiments performed in this temperature range have tested various predictions of the MCT, and agreement has generally been good [5]. Nevertheless, the original idealized version of MCT is known to be incomplete, since the absolute structural arrest and viscosity divergence it predicts at the crossover temperature T_c do not actually occur.

The extended version of MCT includes coupling to current fluctuations [6–10] which represent activated transport (hopping) processes. These terms restore ergodicity below T_c and replace the discontinuous transition of the idealized theory by a smooth crossover from liquid to glassy dynamics, avoiding the viscosity divergence at T_c and the disappearance of both the α-relaxation peak and susceptibility minimum below T_c. However, quantitative data analysis with the extended theory for real materials has not previously been possible since the magnitude of the relevant hopping terms was not known. Consequently, all previous experimental tests of the MCT have been restricted to the idealized version of MCT with the hopping terms neglected.

We recently reported two depolarized-light-scattering studies of the liquid-glass transition, one in the ionic salt calcium potassium nitrate [$CKN,Ca_{0.4}K_{0.6}(NO_3)_{1.4}$] [11], and the second in the molecular glass former Salol [12]. The spectra, spanning over four decades in frequency, were converted to the susceptibility spectra $\chi''(\omega)$ shown in Fig. 1. For comparison with the current analysis, we show the original fits, obtained with the idealized MCT, in Figs. 1(a) and 1(c). Exponent parameters $\lambda=0.81\pm0.05$ for CKN and $\lambda=0.70\pm0.05$ for Salol were obtained from the analyses. The parameter λ governs the universal features of the relaxation process, as will be explained below. The susceptibility spectra revealed the critical slowing down of structural relaxation in the intermediate-frequency β-relaxation region as T_c is approached either from above or below, a central prediction of MCT which had not previously been tested.

Although the quality of the fits was generally good, systematic discrepancies appeared for both materials below and just above T_c at frequencies near the lower limit of our experimental window ($\lesssim 1$ GHz). The discrepancies are particularly visible in the CKN data of Fig. 1(a) at temperatures below 393 K where the theoretical curves tend to fall systematically below the experimental data at low frequencies. Such discrepancies should be expected with the idealized theory in which the minimum in $\chi''(\omega)$ moves to zero and disappears at T_c. When hopping terms are included, the α-relaxation peak will still be present below T_c and the susceptibility spec-

 ©1993 The American Physical Society

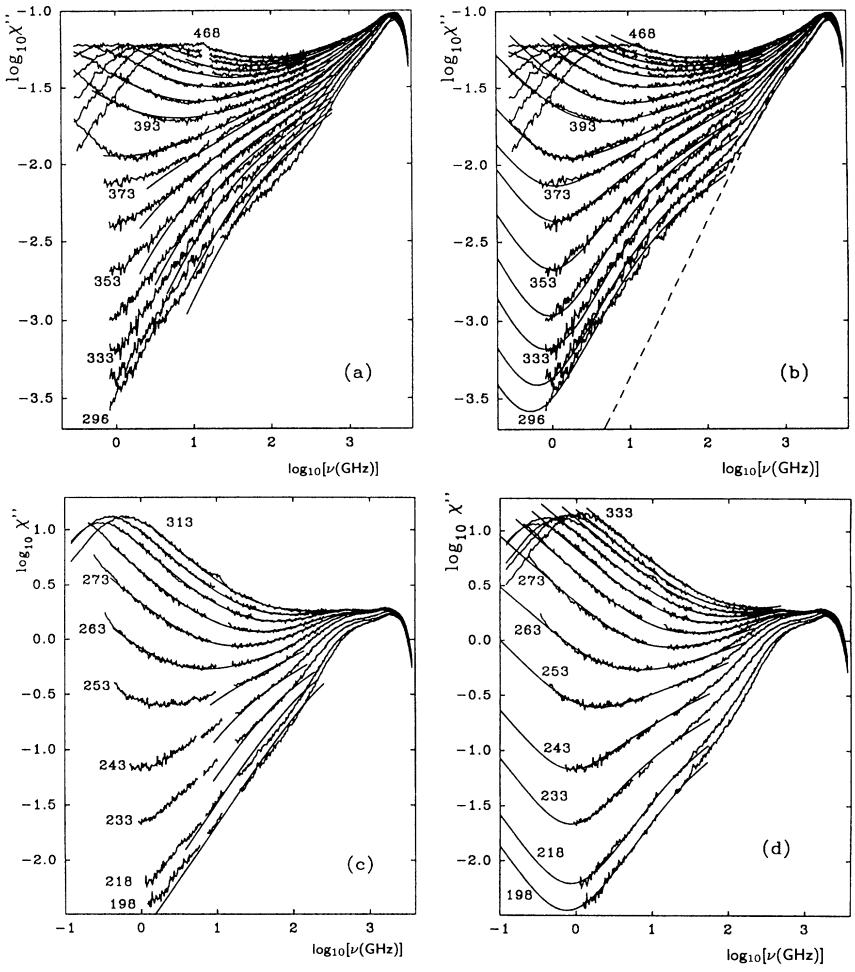

FIG. 1. Susceptibility spectra $\chi''(\omega)$ of CKN, (a), (b), and Salol, (c), (d). The temperatures range from $T=296$ to 468 K for CKN and from $T=198$ to 313 K (c) or $T=333$ K (d) for Salol. The previously published $\delta=0$ idealized MCT fits for CKN with $\lambda=0.81$ and for Salol with $\lambda=0.70$ are shown in (a) and (c), respectively. The solid lines in (b) and (d) are fits with the $\delta\neq 0$ β-relaxation functions of the extended MCT with $\lambda=0.85$ (CKN) and $\lambda=0.73$ (Salol). The dashed line in (b) is an upper limit to the white-noise spectrum $\chi''(\omega)\propto\omega$ matched to the microscopic peak.

tra will therefore continue to show a minimum. Although the spectral range of the data in Fig. 1 does not extend to low enough frequencies to reveal this minimum at temperatures below T_c, its presence is presumably responsible for the fact that the low-frequency experimental data lie above the theoretical curves of the idealized theory.

The presence of these discrepancies provides a means to quantitatively evaluate the magnitude of the hopping terms in the extended MCT. We have therefore carried out an analysis of the CKN and Salol data shown in Fig. 1 with the extended MCT including hopping terms. We have also used the results of this analysis for CKN to predict the form of the intermediate scattering function, and find agreement with the neutron spin-echo data of Mezei [13].

In Sec. II we present a brief review of the idealized and extended versions of the mode-coupling theory to set the stage for the analysis. In Sec. III we describe the new data analysis and give numerical results of the fits to the extended MCT. (Additional details of the fitting procedure are given in Sec. V.) In Sec. IV we utilize the β correlators deduced from the new fits for the CKN light-scattering data to reanalyze the CKN neutron spin-echo data of Mezei, Knaak, and Farago [13,14]. We also discuss the effect of hopping terms on the nonergodicity parameter (or Debye-Waller factor) f_q.

II. THEORETICAL BACKGROUND

In this section we present those mathematical results of the MCT required for our data analysis. We will also review briefly the context within which these results have been derived in the original papers so that the reader gets a self-contained background for our data interpretation.

A. General MCT

The MCT is based on a closed set of nonlinear integrodifferential equations for various correlation functions. The basic one is the correlation function for the density-fluctuation modes $\rho_{\mathbf{q}}(t)$ with wave vectors $\mathbf{q}$:

$$\phi_q(t)=\langle\rho_{\mathbf{q}}^*(t)\rho_{\mathbf{q}}\rangle/\langle|\rho_{\mathbf{q}}|^2\rangle\ . \tag{2.1}$$

Here $q=|\mathbf{q}|$ denotes the wave-vector modulus. The first equation connects accelerations, Hooke's restoring forces, and a generalized friction force:

$$\ddot{\phi}(t)+\Omega_q^2\phi_q(t)+\int_0^t M_q(t-t')\dot{\phi}_q(t')dt'=0\ . \tag{2.2a}$$

This equation can be derived exactly within the Zwanzig-Mori formalism. Its interpretation as a generalized oscillator equation is more obvious if one rewrites it via Fourier-Laplace transformation to one for the frequency-dependent dynamical compressibility $\kappa_q(\omega)$:

$$\kappa_q(\omega)=-(q^2/\rho)/[\omega^2-\Omega_q^2+\omega M_q(\omega)] . \tag{2.2b}$$

The kernel $M_q(\omega)$ is expressed in terms of a Newtonian friction constant v_q and two further kernels $m_q(\omega)$ and $\delta_q(\omega)$:

$$M_q(\omega)=\Omega_q^2[iv_q+m_q(\omega)]/\{1-\delta_q(\omega)\Omega_q^2[iv_q+m_q(\omega)]\} . \tag{2.3}$$

Kernel $m_q(\omega)$ describes the cage effect, i.e., the tendency for the particles to get trapped in cages formed by their neighbors. Kernel $\delta_q(\omega)$ describes hopping transport, i.e., the motion of particles over potential barriers with the assistance of phonons. The two kernels are obtained approximately as correlations for pair modes; pairs of density fluctuations in the case of $m_q(\omega)$ and pairs of densities and currents for $\delta_q(\omega)$. The equations are closed by employing Kawasaki's factorization approximation; essentially one expresses averages of pairs by pairs of averages to obtain:

$$m_q(t)=\tfrac{1}{2}\sum_{k,p} V(q,kp)\phi_k(t)\phi_p(t) , \tag{2.4a}$$

$$\delta_q=\sum_{k,p} V'(q,kp)\phi_k(t)\ddot{\phi}_p(t) . \tag{2.4b}$$

The two frequency scales for the microscopic transient motion Ω_q, v_q and the vertices V, V' are obtained as smooth function of temperature T and density ρ. They can be evaluated with standard approximations invented previously for the theory of simple liquids. Anticipating Ω, v, V, and V' as known, one can in principle solve the equations for the correlators. Actually, the theory for δ_q is more complicated since a complete form of Eq. (2.4b) contains additional terms, e.g., because of couplings to transversal currents. This requires that shear correlations are also considered [7].

B. β relaxation

The idealized MCT deals with the mathematical problem where $V'=0$. One considers the model for dynamics, where activated transport is assumed to be absent. Then one can show that there is some critical temperature T_c so that for $T>T_c$ relaxation towards equilibrium occurs, $\phi_q(t\to\infty)=0$, while for $T\le T_c$ the correlation functions describe spontaneous arrest, $\phi_q(t\to\infty)=f_q>0$. So the solutions of the MCT for $V'=0$, $T\le T_c$ describe ideal glass states in the sense of Edwards and Anderson [15]. The Edwards-Anderson parameter f_q plays the role of a Debye-Waller factor of a disordered solid and is also referred to as the nonergodicity parameter. At the critical point, $T=T_c$, the Debye-Waller factor is nonzero: $f_q^c=f_q|_{T=T_c}>0$. The parameter points $V(T=T_c)=V^c$, $V'=0$ are called glass-transition singularities (GTS).

The critical Debye-Waller factor is given by the vertices $V(q,kp)$ calculated for $T=T_c$, and so is another quantity $h_q>0$ called the critical amplitude. Furthermore, one calculates from the vertices the exponent parameter λ which fixes two exponents: the critical exponent $0<a\le 0.395\ldots$ and the von Schweidler exponent $0<b\le 1$. For the leading-order long-time relaxation at the singularity ($V=V^c, V'=0$) one finds the critical decay:

$$\phi_q(t\to\infty)-f_q^c=h_q(t_0/t)^a+O((t_0/t)^{2a}) . \tag{2.5}$$

Here there enters a time scale t_0, to be determined by matching the asymptotic law Eq. (2.5) to the microscopic transient motion.

The extended MCT acknowledges that $V'\neq 0$. In this case spontaneous arrest is impossible; the correlators relax to zero, provided one waits long enough. For small enough V' the whole relaxation process for $T\sim T_c$ outside the short-time transient regime consists of two steps. The first one, referred to as β relaxation, describes the decay towards f_q^c and then the motion where $\phi_q(t)$ starts to fall below f_q^c. The second one, referred to as α relaxation, describes the decay from the value f_q^c, where the cage effect tends to arrest the fluctuations, to zero. The α process leads to the well-known α peak in the susceptibility spectra like $\kappa_q''(\omega)$. Figure 1 exhibits these α peaks clearly, within the frequency window of our instrument, for $T>400$ K for CKN and $T>300$ K for Salol. In this paper we will not consider the α process and will deal exclusively with the β dynamics.

The dynamics of the β regime is governed by the underlying glass-transition singularity. It deals with parameters where hopping effects are not too large, $V'\sim 0$, and where the cage effect drives the density fluctuations close to arrest; $V\sim V_c$. The time has to be long enough so that details of the phonon motion are damped out, but short enough so that generalized diffusion processes have not yet allowed the particles to leave their cages irreversibly. The β dynamics describes the susceptibility spectra for frequencies below the band of molecular vibrations. For our examples we found [11,12] the β regime to be located below about 500 GHz [Figs. 1(a) and 1(c)]. The β process also describes the high-frequency wing of the α process and it terminates somewhere above the α-peak position. In our cases the β process shall be used to analyze spectra within frequency windows extending up to three orders of magnitude (see Fig. 1). It is the goal of this analysis to explain variations of the spectral intensity over about three decades as caused by variations of the temperature above T_g. Within the β regime the equation of motion (2.1)–(2.4) can be simplified using $[\phi_q(t)-f_q^c]/h_q=\delta\phi_q(t)$ as a small parameter. One finds as a generalization of Eq. (2.5), in leading order in $\delta\phi_q(t)$, the factorization property

$$\phi_q(t)-f_q^c=h_q G(t) . \tag{2.6a}$$

The dependence of the correlations on time and wave vector are decoupled. There appears no critical variation of physical quantities as a function of distance or wave vector. All the sensitive dependence of the correlators on time and temperature is expressed by one common func-

tion $G(t)$, called the β correlator. Fourier cosine transform yields the β spectrum $G''(\omega)$ and the β-susceptibility spectrum $\chi''(\omega)=\omega G''(\omega)$. The latter determines the compressibility spectra for all q up to an amplitude factor: $\kappa_q''(\omega)=h_q\chi''(\omega)$. Within the MCT, the factorization property is generalized to arbitrary correlation functions of variables X such as stresses, dipole moments, etc. One finds

$$\phi_X(t)-f_X^c=h_X G(t) . \tag{2.6b}$$

The specifications of X merely enter the critical value of the nonergodicity parameter f_X^c and the critical amplitude h_X. The time and sensitive $(T-T_c)$ dependence is given by the same β correlator as before.

A side remark concerning the relevance of Eq. (2.6b) might be in order. In our depolarized-light-scattering experiments we measure the intensity spectrum $I(\omega)\propto\phi_X''(\omega)$ for a variable X, which refers to fluctuations of the electronic part of the dielectric constant. This function has been evaluated previously as a dipole-induced-dipole (DID) scattering function with the result [16]

$$\phi_X(t)=\sum_{k,p} W(k,p)\phi_k(t)\phi_p(t) . \tag{2.7}$$

This is a typical mode-coupling-theory formula, which should be viewed as the analog of Eq. (2.4a). If one substitutes $\phi_q(t)$ from Eq. (2.6a) in the DID formula [Eq. (2.7)], one finds that, within the β-relaxation region, the dominant contribution to the light-scattering spectrum corresponds to an effective susceptibility

$$\chi_{\rm ls}''(\omega)=h_{\rm ls}\chi''(\omega) . \tag{2.8a}$$

Here $\chi''(\omega)$ is the β susceptibility and the amplitude follows as

$$h_{\rm ls}=2\sum_{k,p} W(k,p)f_k^c h_p . \tag{2.8b}$$

All microscopic details boil down to the frequency-independent prefactor $h_{\rm ls}$. If the microscopic theory for the light-scattering process were improved, e.g., by accounting for higher-order products of density fluctuation in Eq. (2.7), the result of Eq. (2.8b) would still be valid. There would merely be a different relation between $h_{\rm ls}$ and f_k^c, h_p.

The β correlator G depends on the large number of coupling constants $V(q,kp)$ and $V'(q,kp)$ via two relevant control parameters only. The separation parameter σ is given by V and specifies the cage effect; it is a smooth function of temperature and its zero defines the critical temperature. Close to the critical point one can write $\sigma=C(T_c-T)/T_c$ with $C>0$. The hopping parameter $\delta>0$ describes the sensitive effect of the activated transport on the β spectra near the glass-transition singularity:

$$G(t)=g(t/t_0,\sigma,\delta t_0) . \tag{2.9}$$

Because of Eq. (2.5) one gets the critical decay law at the glass-transition singularity. The latter is located at the origin of the $(\sigma,\delta t_0)$ parameter plane:

$$g(t/t_0,\sigma=0,\delta t_0=0)=(t_0/t)^a . \tag{2.10}$$

The complete functional form for g is determined by the exponent parameter λ. Let us emphasize that λ (and hence the function g), σ, h_X, and f_X^c are equilibrium constants given solely by the system's structure factor $S(q)$. The matching parameter t_0 and the hopping parameter δ are numbers not expressible in equilibrium quantities only. The connection of all the mentioned parameters with the vertices V,V' is rather involved as can be inferred from the quoted literature [5]. Since we cannot calculate V,V' for the realistic systems under study, we treat the parameters as fit constants.

C. Idealized theory for the β process

Analysis of the MCT equations in the idealized version, where activated hopping processes are neglected, has shown that the β correlator $G(t)$ obeys the equation of motion

$$\sigma+\lambda G^2(t)=\frac{d}{dt}\int_0^t G(t-t')G(t')dt' . \tag{2.11}$$

The exponent parameter λ ($\frac{1}{2}\le\lambda<1$) in Eq. (2.11) is the only free parameter in the idealized MCT. Once λ is specified, Eqs. (2.6) and (2.11) determine the full structure of $\phi_q(t)$ in the intermediate-time regime, apart from the numerical values of f_q^c and h_q. λ, in turn, fixes the two exponents of MCT: the critical exponent a and the von Schweidler exponent b (see Ref. [17] for a table relating a and b to λ). $G(t)$ has also been shown to obey the scaling relation

$$G(t)=C_\sigma g_\pm(t/t_\sigma),\quad \sigma\gtrless 0 , \tag{2.12}$$

where the amplitude scale C_σ and time scale t_σ are given by

$$C_\sigma=|\sigma|^{1/2},\quad t_\sigma=t_0(|\sigma|)^{-1/2a} . \tag{2.13}$$

For a given λ, the β correlators $G(t)$ at different temperatures are self-similar and are all determined by the two master functions $g_\pm(t/t_\sigma)$ via Eq. (2.12). The corresponding susceptibility master functions $\chi_\pm''(\omega)$ for the susceptibility $\chi''(\omega)$, where

$$\chi''(\omega)=\omega\int_0^\infty\cos(\omega t)G(t)dt \tag{2.14}$$

can be constructed by solving Eq. (2.11) numerically, or by using the power-law expansions and tables of coefficients in Ref. [17]. The $\chi_\pm''(\omega)$ master curves for $\lambda=0.70$ were used in Ref. [12] to find the theoretical susceptibility functions

$$\chi_q''(\omega)=h_q|\sigma|^{1/2}\chi_\pm''(\omega/\omega_\sigma) \tag{2.15}$$

for Salol shown in Fig. 1(c). Equations (2.12)–(2.15) were the basis of the data analysis for the β-relaxation region in all previous experiments, including our light-scattering studies of CKN [11] and Salol [12] where an extensive discussion of the fitting procedure can be found.

D. Extended theory for the β process

In the extended MCT, the correlation function $\phi_q(t)$ still obeys Eq. (2.6) in the β-relaxation region. The β

correlator $G(t)$ is no longer determined by Eq. (2.11), however, but by its generalization [7,10]

$$\sigma-\delta t+\lambda G^2(t)=\frac{d}{dt}\int_0^t G(t-t')G(t')dt \ . \tag{2.16}$$

Note that the hopping term δt in Eq. (2.16) guarantees that at sufficiently long times $\phi_q(t)$ cannot arrest in an ideal glass state.

In the extended MCT, $G(t)$ depends on both the separation parameter σ and the hopping rate δ. Upon changing the temperature, the relevant parameters move along a trajectory C in the $(\sigma,\delta t_0)$ plane: $T\rightarrow(\sigma(T),\delta(T))$. For a general trajectory C the *form* of $G(t)$ will change with temperature, in contrast to the horizontal trajectory $\delta t_0=0$ of the idealized MCT where the one-parameter scaling relation Eq. (2.12) applies. Thus, for a given λ, the form of $G(t)$ must be found for each pair $(\sigma,\delta t_0)$ by solving Eq. (2.16) [10]. The analysis is simplified considerably by the fact that $G(t)=g(t/t_0,\sigma,\delta t_0)$ of Eq. (2.16) obeys a two-parameter scaling law [7]:

$$g(yt/t_0,\sigma/y^{2a},\delta t_0/y^{1+2a})=y^{-a}g(t/t_0,\sigma,\delta t_0) \tag{2.17}$$

for arbitrary $y>0$.

Equation (2.17) implies that the form of $G(t)$ is self-similar along any scaling line, passing through the arbitrary point $(\hat{\sigma},\hat{\delta}t_0)$ in the $(\sigma,\delta t_0)$ plane, where the scaling line is defined by

$$(\sigma,\delta t_0)=(\hat{\sigma}y^{2a},\hat{\delta}t_0y^{1+2a}) \ , \tag{2.18}$$

with $y>0$ denoting the line parameter. As $y\rightarrow 0$, all scaling lines, which have the form of generalized parabolas $\delta t_0=c|\sigma|^{(1+2a)/2a}$, approach the GTS at (0,0). (Each scaling line corresponds to a particular value of the constant c.) Several such scaling lines are shown in Figs. 3 and 5, to be discussed in the following section. Note that each generalized parabola actually corresponds to two different master functions: one for the left side ($\sigma<0$, liquid), and another for the right side ($\sigma>0$, glass).

A similar scaling law applies to the susceptibility spectra:

$$\chi''(y\omega t_0,\hat{\sigma}y^{2a},\hat{\delta}t_0y^{1+2a})=y^a\chi''(\omega,\hat{\sigma},\hat{\delta}t_0) \tag{2.19}$$

so that a $\log(\chi'')$-$\log(\omega)$ plot for $(\hat{\sigma}y^{2a},\hat{\delta}t_0y^{1+2a})$ has exactly the same form as that for $(\hat{\sigma},\hat{\delta}t_0)$, except that is is shifted by $\log(y)$ along the horizontal axis and by $\log(y^a)$ along the vertical axis. Thus the data analysis for $\chi''(\omega)$ can proceed in two steps. First, for a particular λ and fixed hopping rate, e.g., $\hat{\delta}t_0=1$, one looks for a separation parameter $\hat{\sigma}$ for which the shape of the experimental $\log(\chi'')$-$\log(\omega)$ curve is reproduced. This fixes the relevant scaling line. Then the value of y in Eq. (2.18) is adjusted until the two curves overlap, which identifies the point $(\sigma,\delta t_0)$.

An alternative procedure, which was used in the data analysis described in the next section, follows from the observation that the dimensionless hopping rate δt_0 introduces a natural scale σ_0 for the separation parameter σ [7],

$$\sigma_0=(\delta t_0)^{(2a)/(1+2a)} \ . \tag{2.20}$$

We can define σ^* as the separation parameter σ measured in its natural units σ_0 of Eq. (2.20),

$$\sigma^*=\sigma/\sigma_0 \ . \tag{2.21}$$

Equations (2.19) and (2.20) show that every scaling line corresponds to a particular value of σ^*. One can thus vary λ and σ^* until the theoretical and experimental $\log(\chi'')$-$\log(\omega)$ curves are as similar in shape as possible, and then choose σ and the amplitude prefactor h of Eq. (2.6) to produce as complete overlap as possible between the two curves.

Finally, we note that the correlators and susceptibility spectra in the region of the β process are expected to evolve smoothly from the liquid ($\sigma\ll-\sigma_0$) to the transition region ($-\sigma_0\leq\sigma\leq\sigma_0$) to the glass ($\sigma\gg\sigma_0$). In contrast to the predictions of the idealized theory there is no abrupt change in $G(t)$ or $\chi''(\omega)$ at $T=T_c$.

III. DATA ANALYSIS

A. CKN

CKN ($T_g\cong 333$ K, $T_m\cong 438$ K) susceptibility spectra in the range 296–468 K, found from the depolarized-light-scattering spectra, are shown in Fig. 1(a) along with the theoretical fits to the idealized ($\delta=0$) theory with $\lambda=0.81$ reported in Ref. [11]. Obviously it is advisable to start data analysis by using the idealized MCT. However, in doing so one should make sure that the identified discrepancies between data and formulas have the qualitative trends to be expected due to $\delta\neq 0$ effects. For example, the critical spectrum $\chi''\propto\omega^a$ should be most evident for $T=T_c$. Therefore one has to fit this part of the spectrum as was done for CKN for $T=373$ K in Fig. 1(a). It would be incorrect to force the theoretical curve to match the data for $\nu=1$ GHz. These 1-GHz data show the expected precursors of the $\delta\neq 0$ induced minimum and therefore they must not follow the $\delta=0$ MCT results.

Figure 1(b) shows the same $\chi''(\omega)$ data with the new extended MCT fits. The dashed line is a white-noise spectrum $\chi''(\omega)\propto\omega$ matching the microscopic band at 3 THz. The enhanced signal above this white-noise background, in the region between the α peak and the microscopic peak, is due to the β-relaxation process. The solid lines in Fig. 1(b) are the new extended MCT results obtained by solving Eq. (2.16). The fits were carried out for λ in the range determined by the $\delta=0$ fits ($0.76<\lambda<0.86$) with arbitrarily chosen $t_0=(1/2\pi)$ ps. The fitting procedure, described at the end of the preceding section, led to an exponent parameter $\lambda=0.85$. The corresponding critical exponents are $a=0.25$, $b=0.39$, $\gamma=3.3$. Changing λ by ± 0.02 gave fits of similar quality. The resulting fit parameters h, σ, and δ are listed in Table I. The separation parameter σ and the scale σ_0 [from Eq. (2.20)] for each spectrum are shown in Fig. 2(a), and the amplitudes $h=h_{\rm ls}$ are shown in Fig. 2(b).

In Fig. 3 we show the $(\sigma,\delta t_0)$ points (open circles) found for each spectrum in the $(\sigma,\delta t_0)$ plane along with a series of scaling lines. The solid scaling curve (second

from the inside) corresponds to $\sigma=\sigma_0$, i.e., to $\sigma^*=1$. The heavy line C through the data points, to be described below, is the trajectory C followed by the system in the $(\sigma,\delta t_0)$ plane. From the intersections of the $\sigma=\pm\sigma_0$ scaling line and the trajectory C, we see that the transition region extends approximately from 363 to 403 K.

In Figs. 2 and 3, uncertainties in the parameter values found in the fits are indicated by error bars at three temperatures: 423, 383, and 333 K. They were estimated by changing σ^* as much as possible while adjusting σ, σ_0, and h to find an acceptable fit. The errors estimated in this way are not independent; it is not possible, e.g., to select in Fig. 3 the lower bound for σ and the upper bound for δt_0 and still obtain an acceptable fit. The various fit parameters are correlated. One cannot exhaust the error margins for σ, σ_0 (i.e., δ), and h, indicated, e.g., in Fig. 2 for $T=423$ K arbitrarily, without ruining the fit quality. The indicated error bar, e.g., for σ is meant as follows: we could choose σ anywhere within this bar and get a fit of similar quality as that shown in Fig. 1, *provided* that the other parameters were also changed properly. Because of the scaling law Eq. (2.17), the value for t_0 is arbitrary. One could change t_0, even by a T-dependent factor, provided one would change h, σ, and δ as given in Eq. (2.17). In this way one could scale, for example, the amplitude h_{ls} to a temperature-independent number. We have not examined whether T-dependent choices of t_0 lead to results for σ, δ, and h which look more plausible than the ones shown. Neither did we try to improve the fits by choosing a temperature-dependent exponent parameter λ.

At the highest temperatures ($T\geq 433$ K) the susceptibility spectra were found to have a T-independent shape [11]. No improvement in the fit could be found by taking $\delta t_0\neq 0$, so the upper four theoretical curves for $T\geq 433$ K in Fig. 1(b) were found from the idealized MCT. Below 423 K, the difference in shape between the experimental spectra and theoretical spectra of the idealized MCT becomes increasingly evident at frequencies below ~ 1 GHz. At 383 K, which is ~ 5 K above the $T_c=378$ K found in Ref. [11], the low-frequency discrepancy has become severe and cannot be improved within the idealized $\delta=0$ MCT.

For $T<T_c$, the idealized MCT predicts a knee in the susceptibility spectrum at a frequency ω_e where an abrupt crossover occurs from the critical spectrum $\chi''(\omega)\propto\omega^a$ for $\omega>\omega_e$ to $\chi''(\omega)\propto\omega$ (white-noise spectrum) for $\omega<\omega_e$. This abrupt change is not observed for the CKN data; even for $T=296$ K the ω^a to ω^1 crossover is rather smooth. All these deficiencies of the idealized

TABLE I. Fitting parameters for extended MCT analysis ($t_0=1/2\pi$ ps).

T (K)	σ	δt_0	h
	CKN		
296	5.75×10^{-2}	3.64×10^{-7}	3.48×10^{-2}
318	5.75×10^{-2}	5.45×10^{-7}	4.19×10^{-2}
333	5.75×10^{-2}	9.09×10^{-7}	5.53×10^{-2}
343	5.13×10^{-2}	1.29×10^{-6}	6.86×10^{-2}
353	3.14×10^{-2}	2.20×10^{-6}	6.65×10^{-2}
363	1.94×10^{-2}	3.44×10^{-6}	7.98×10^{-2}
373	7.35×10^{-3}	3.68×10^{-6}	8.85×10^{-2}
383	-8.88×10^{-4}	6.29×10^{-6}	9.23×10^{-2}
393	-2.06×10^{-2}	1.64×10^{-5}	9.73×10^{-2}
403	-3.25×10^{-2}	3.25×10^{-5}	1.08×10^{-1}
413	-5.13×10^{-2}	5.15×10^{-5}	1.12×10^{-1}
423	-7.39×10^{-2}	3.88×10^{-5}	1.11×10^{-1}
433	-9.08×10^{-2}		1.11×10^{-1}
443	-1.02×10^{-1}		1.14×10^{-1}
453	-1.14×10^{-1}		1.15×10^{-1}
468	-1.31×10^{-1}		1.13×10^{-1}
	Salol		
198.2	8.57×10^{-2}	8.54×10^{-7}	0.483
218.2	7.41×10^{-2}	1.17×10^{-6}	0.610
233.2	3.16×10^{-2}	1.93×10^{-6}	0.892
243.2	1.31×10^{-2}	2.62×10^{-6}	1.39
253.2	-4.09×10^{-3}	6.40×10^{-6}	2.09
263.2	-2.69×10^{-2}	8.52×10^{-6}	2.66
273.2	-5.32×10^{-2}	4.69×10^{-5}	3.04
283.2	-8.32×10^{-2}	1.11×10^{-4}	3.27
293.2	-1.32×10^{-1}	1.05×10^{-4}	3.27
303.2	-1.84×10^{-1}		3.14
313.2	-2.36×10^{-1}		3.01
323.2	-2.64×10^{-1}		3.08
333.2	-3.24×10^{-1}		2.88

MCT are caused by taking $\delta \neq 0$; fitting these features in the extended MCT allows δ to be determined rather precisely.

For $343 < T < 413$ K the separation parameter σ shown in Fig. 2 was found to vary linearly with temperature as discussed in Sec. II B. A least-squares fit to $\sigma \propto (T_c - T)/T_c$ yielded $T_c = 378 \pm 1$ K, in agreement with our previous estimate [11]. Since in the extended MCT the hopping rate δ results from activated processes [9], the temperature dependence of δt_0 found from the fits was interpolated with an Arrhenius law

$$\delta t_0 = C_0 \exp(-E/RT) . \tag{3.1}$$

Optimizing the fits for $343 < T < 413$ K gave $E = 294$ kcal/mol and $C_0 = 37\,568$, i.e., $\delta t_0(T_c) = 6.3 \times 10^{-6}$. The linear fit for σ and the Arrhenius fit for δt_0 were used to construct the trajectory C shown in Fig. 3. The result is similar to a previous conjecture [8] based on estimates of δt_0.

The critical amplitude $h_{ls}(T)$ shown in Fig. 2(b) exhibits no anomaly near T_c, in contrast to the result of our analysis based on the idealized MCT [12]. For $343 < T < 413$ K a linear interpolation, shown in Fig. 2(b), gave

$$h_{ls} = (0.089 \pm 0.001) + (0.25 \pm 0.02)(T_c - T)/T_c . \tag{3.2}$$

For $T > 413$ K and $T < 343$ K the data deviate from this linear behavior indicating that further correction terms to the leading asymptotic formula $h_{ls} = \text{const}$ become significant for $|T - T_c| \geq 40$ K.

Let us reiterate the contents of Figs. 2 and 3. With increasing T the hopping rate δt_0 increases rapidly; but the scaling lines increase even more rapidly. For $\sigma = -\sigma_0$,

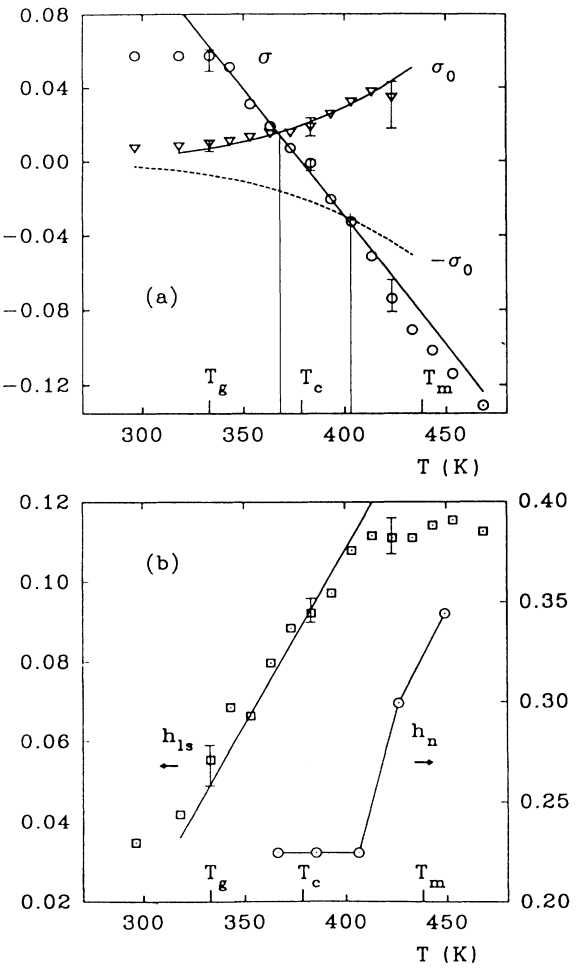

FIG. 2. The parameters for the extended β-theory fits of Fig. 1(b) to the CKN data as functions of temperature. (a) The separation parameter σ and the hopping-induced scale σ_0. The microscopic matching parameter t_0 is arbitrarily chosen to be $2\pi t_0 = 1$ ps. The straight line is a linear fit $\sigma^f = A(T_c - T)/T_c$ to σ in the temperature range $343 \leq T \leq 413$ K, with $T_c = 378.5$ K and $A = 0.52$. The solid and dotted lines are Arrhenius fits to σ_0 (respectively, $-\sigma_0$) in the same temperature range: $\sigma_0^f = 32.9 \exp(-2806/T)$. Error bars for the temperatures $T = 333$, 383, and 423 K indicate estimates for the uncertainties in choosing the fits of Fig. 1(a). The vertical lines at $T = 368$ and 403 K are the boundaries of the transition region where $|\sigma| < \sigma_0$. (b) Comparison of the critical amplitudes h_{ls} (left axis) and h_n (right axis) used in the fits to the light-scattering or to the neutron-scattering data of CKN. The solid line through h_{ls} is a linear fit in the temperature range $343 \leq T \leq 413$ K; $h_{ls} = 0.089 + 0.25(T - T_c)/T_c$. Error bars for the temperatures $T = 333$, 383, and 423 K are estimated from the fits of Fig. 1(b).

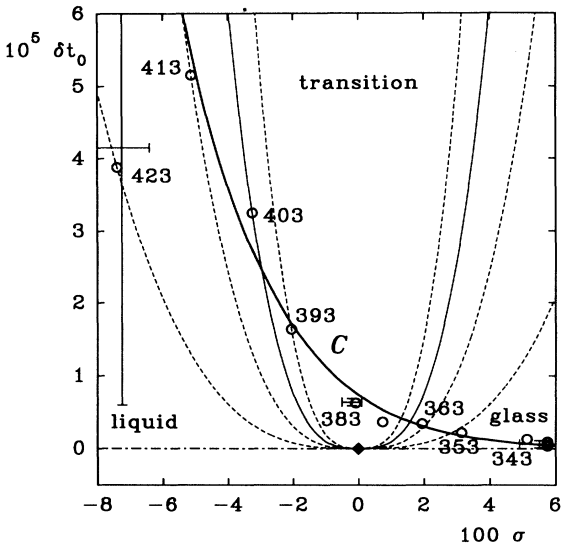

FIG. 3. Control parameter space explored by CKN in the temperature range $296 \leq T \leq 423$ K. For $433 \leq T \leq 468$ K, $\delta = 0$ can be chosen. The data points are obtained from the fits of Fig. 1(b). Error bars in σ and δ at $T = 333$, 383, and 423 K are estimated by visually comparing different fits. The bold solid line giving the approximate path C in parameter space corresponds to the Arrhenius and linear fits of Fig. 2(a). The four generalized parabolas are scaling lines with $\sigma/\sigma_0 = \pm 2.15$, ± 1.36, ± 1, and ± 0.79 (listed by increasing steepness). They join in the glass-transition singularity at $(\sigma, \delta) = (0,0)$ marked by a diamond, which also separates the idealized liquid ($\sigma < 0, \delta = 0$) from the idealized glass ($\sigma > 0, \delta = 0$) scaling lines, both shown as chain curves.

i.e., for $T \sim 403$ K, the trajectory C leaves the δ-dominated transition region. For higher temperatures the scaling lines correspond to master functions which are nearly indistinguishable from those of the idealized theory. Despite δ being large, it can be ignored for $T > 433$ K. Of course for too large $(T - T_c)$ corrections to the scaling laws will invalidate the basic equation (2.6).

With decreasing T, the edge of the transition region $\sigma = +\sigma_0$ is reached for $T \sim 363$ K. The master functions at high frequencies are close to those of the idealized MCT which accounts for the increase of the relative uncertainty in our determination of δ at low temperatures. However, for $T < T_c$, the low-frequency spectra are qualitatively different from those of the idealized MCT in that they continue to predict a minimum. The major shortcoming of the idealized MCT is that it fails to correctly describe the low-frequency spectrum at and below the most interesting temperature $T = T_c$. The present analysis, in contrast, has the largest range of validity for $T = T_c$ [10].

Additional details of the fitting of the CKN data and the influences of activated hopping processes will be presented in Sec. V.

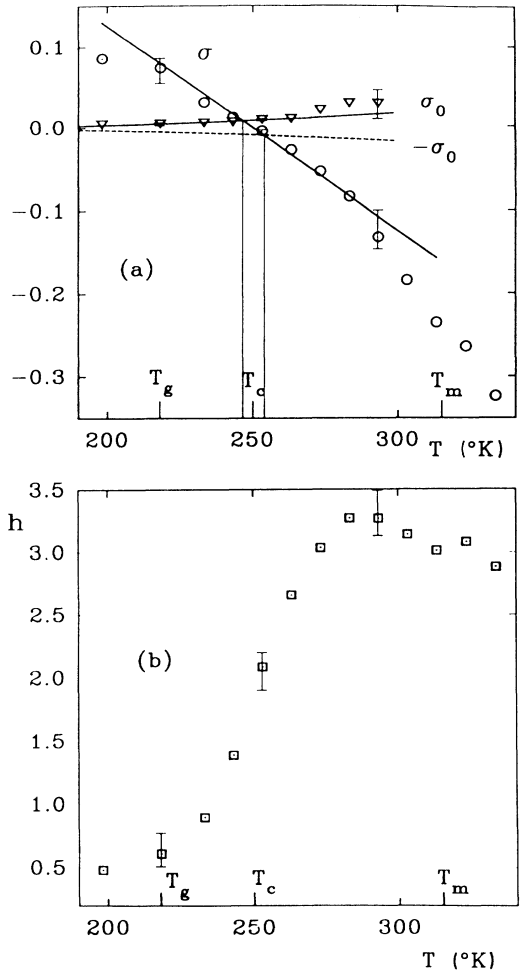

FIG. 4. The parameters of the extended β-theory fits of Fig. 1(d) with $\lambda = 0.73$, $\delta \neq 0$ to the Salol data. (a) The separation parameter σ and the hopping-induced scale σ_0. The microscopic matching parameter t_0 is chosen to be $2\pi t_0 = 1$ ps. The straight line is a linear fit $\sigma^f = A(T_c - T)/T_c$ to σ in the temperature range $218 \leq T \leq 283$ K, with $T_c = 250$ K and $A = 0.625$. The solid and dotted lines are Arrhenius fits to σ_0 (respectively, $-\sigma_0$) for T below T_c; $\sigma_0^f = 0.51 \exp(-1017/T)$. Error bars for the temperatures $T = 218$, 253, and 293 K indicate the uncertainties in the fits of Fig. 1(c). The vertical lines at $T = 245$ and 255 K enclose the transition region where $|\sigma| < \sigma_0$. (b) The critical amplitude h used in the fits of Fig. 1(c). Error bars for the temperature $T = 218$, 253, and 293 K are estimated from the fits of Fig. 1(c).

B. Salol

The $\chi''(\omega)$ spectra of Salol ($T_g = 218$ K, $T_m = 315$ K) for $198 < T < 333$ K reported in Ref. [12] are shown in Figs. 1(c) and 1(d). The theoretical curves in 1(c) are the idealized MCT predictions with $\lambda = 0.70$ which were discussed previously [12]. The generalized MCT analysis, which followed the same procedures described above for CKN, led to $\lambda = 0.73$, and produced the theoretical spectra shown in Fig. 1(d). The reliability of the fits is more restricted than for CKN due to the low-lying microscopic excitations near 400 GHz.

At high temperatures, λ is primarily determined by the low-frequency (von Schweidler) wing which seems to ex-

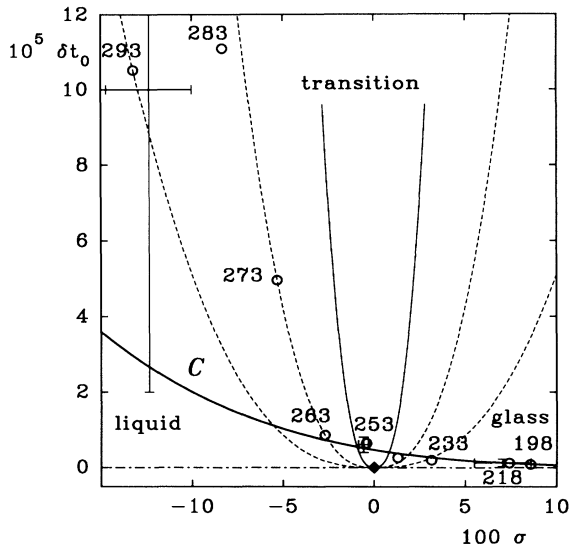

FIG. 5. Control parameter space explored by Salol in the temperature range $198 \leq T \leq 293$ K. For $303 \leq T \leq 333$ K, $\delta = 0$ can be chosen. The data points are obtained from the fits of Fig. 1(d). Error bars at 218, 253, and 293 K are estimated by visually comparing different fits. The bold solid line giving the approximate path C in parameter space corresponds to the Arrhenius and linear fits of Fig. 4(a). The three generalized parabolas are scaling lines with $\sigma/\sigma_0 = \pm 4.52$, ± 2.43, and ± 1 (listed by increasing steepness). They join in the glass-transition singularity at $(\sigma, \delta) = (0, 0)$ marked by a diamond, which also separates the idealized liquid $(\sigma < 0, \delta = 0)$ from the idealized glass $(\sigma > 0, \delta = 0)$ scaling lines, both shown as chain curves.

tend up to the maximum of the α peak. The high-frequency part of the β spectrum is not visible for $T > 313$ K due to the broad microscopic excitations. For lower temperatures ($263 < T < 303$ K) the spectra do not extend more than one-half decade above the minimum, which is not enough to exhibit the critical ω^a behavior. Only the 253-K spectrum appears to exhibit both ω^a and ω^{-b} regions, and even here the spectrum extends less than one decade below the minimum.

The extended MCT analysis, described in more detail in Sec. V, led to a crossover temperature $T_c = 250$ K, somewhat lower than the value $T_c = 256$ K found in our original analysis [12]. For $T < T_c$, the split microscopic band prevents the observation of the characteristic knee in the spectrum which marks the crossover from $\chi''(\omega) \propto \omega^a$ to $\chi''(\omega) \propto \omega$. Therefore the uncertainty in the fits for $T < 250$ K and the estimates of the minima in Fig. 1(d) is higher than that for CKN.

Figure 4(a) shows the values of σ and σ_0 found from the fits, while Fig. 4(b) displays the results for h. In Fig. 5 we show the trajectory C in the $(\sigma, \delta t_0)$ plane, found by the same procedure described above for CKN, along with several scaling lines. Because σ_0 is much smaller for Salol than for CKN, the transition region is very narrow. In fact, as seen in Fig. 5, only the $T = 253$ K point falls within the transition region.

IV. RELATION TO NEUTRON SPIN-ECHO SPECTROSCOPY

A. The intermediate scattering function

Inelastic neutron-scattering spectroscopy employing spin-echo and time-of-flight techniques permits direct determination of $\phi_q(t)$ which is usually assumed to be equivalent to the normalized intermediate scattering function. Such experiments have provided the principal experimental tests of MCT and have the great advantage of permitting the experimenter to select the value of q. In this manner one can also explore correlations in space.

A neutron spin-echo study of CKN by Mezei, Knaak, and Farago in 1987 [14] determined $\phi_q(t)$ for q near the peak of the static structure factor $S(q)$ in the range 4×10^{-11} s $\le t \le 2\times10^{-9}$ s for temperatures between 384 and 469 K. Assuming that the data fell entirely within the α-relaxation region, they fit it to the Kohlrausch function

$$\phi_q(t) = f_q \exp[-(t/\tau)^\beta] \ . \tag{4.1}$$

[The idealized MCT indicates that Eq. (4.1) is usually a good approximation to the major part of the α process [18,19].] They found that all the data could be fit with a single $f_q = 0.84$ and $\beta = 0.58$, in agreement with the scaling (or time-temperature superposition) principle required by MCT for $T > T_c$. By combining this spin-echo data with time-of-flight data, Knaak, Mezei, and Farago [20] attempted to demonstrate the existence of two power-law regions in $\phi_q(t)$ and of a minimum in $\chi''(\omega)$ as predicted by MCT.

Subsequently, Mezei [13] reported extended CKN neutron spin-echo measurements covering the range 2×10^{-12} s $\le t \le 1\times10^{-9}$ s for temperatures between 366 and 560 K. Part of the data are reproduced in Fig. 6(a). For this extended set of data spanning nearly three decades in time, Mezei found that fits to Eq. (4.1) with fixed f_q were no longer successful. The fits suggested a

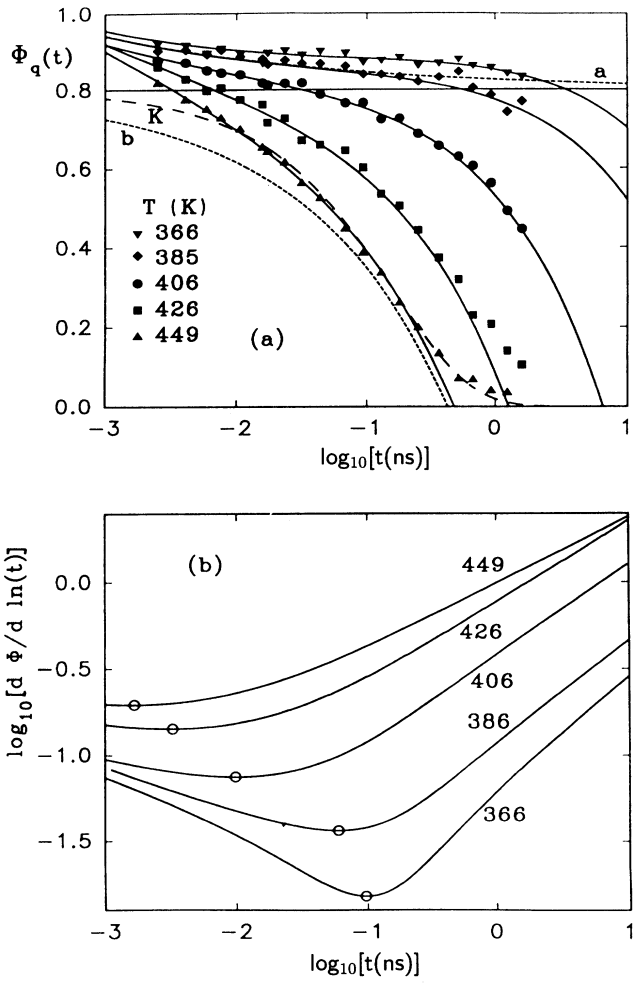

FIG. 6. This figure demonstrates the factorization property of Eq. (2.6) for neutron spin-echo data in CKN and the β-relaxation fits of Fig. 1(b). (a) CKN neutron-scattering data at the peak of the static structure factor for the five temperatures (from Ref. [13]) and the β-relaxation fits with parameters taken from the analysis of the susceptibility spectra [Fig. 1(b)]. Resulting values of h_n are shown in Fig. 2(b). The horizontal line is the constant nonergodicity parameter $f^c_{q_0} = 0.80$ used for the β-relaxation fits (solid lines). The dotted line marked a is the critical correlator corresponding to the fit at $T = 385$ K closest to T_c. The dotted line marked b is the von Schweidler asymptote of the $\lambda = 0.85$, $\delta = 0$ master curve for $T = 449$ K. The dashed curve marked K is a Kohlrausch fit $Ae^{-(t/\tau)^\beta}$ to the $T = 449$ K data with fixed amplitude $A = f^c_{q_0}$ and fitted $\beta = 0.71$ and $\log_{10}[\tau(\text{ns})] = -0.80$. (b) Double logarithmic plot of the derivative of the correlator $\phi_q(t)$ with respect to the logarithm of time $\log_{10}(t)$. The fitted β correlators of (a) are taken corresponding to the temperatures $T = 449$, 426, 406, 386, and 366 K from top to bottom. The open circles show the locations of the minima.

marked temperature dependence for the Kohlrausch exponent β, in disagreement with the scaling prediction of MCT. Mezei noted that this disagreement could result from the presence of both α- and β-relaxation processes within the experimental time window which would invalidate fits of the data to Eq. (4.1).

Our analysis of the CKN depolarized-light-scattering data has determined the β correlator $G(t)$ in Eq. (2.6b). This result can now be substituted in (2.6a) to predict the neutron-scattering function $\phi_q(t)$ in the β region. Notice that the complete time dependence and the sensitive temperature dependence are given by the data in Table I. Only f_q^c and h_q are treated as fit parameters, which may be smoothly temperature dependent.

The result of this fitting procedure is shown in Fig. 6. The neutron data points at five temperatures are plotted together with the fit results, shown as solid lines. The fits gave $f_q^c=0.80\pm0.01$. The amplitude $h_q(T)$, shown in Fig. 2(b) by h_n, increases smoothly with temperature as found above for $h_{\rm ls}$. The fits show no deviations at short times due to fast microscopic motions, indicating that for the range of temperatures shown, $\phi_q(t)$ has already entered the β-relaxation region by $t=2\times10^{-12}$ s. For the 385-K data which are the closest to T_c, the critical decay [Eq. (2.5)] is shown by the broken line marked *a*. The agreement with the data shows that the short-time decay of $\phi_q(t)$ cannot belong to the α process, as noted by Mezei [13].

For the highest-temperature data (449 K) shown in Fig. 6, the von Schweidler decay, $\Phi_q(t)-f_q^c\propto -t^b$ [5], for $\lambda=0.85$ and $\delta=0$, computed as an asymptote to the master function, is indicated by the dashed line marked *b*. Only for the two highest temperatures (449 and 426 K), at the longest times, does $\phi_q(t)$ deviate noticeably from the prediction of Eq. (2.6a). This deviation is due to the α process which is not treated in the present discussion. The dashed line marked *K* is a Kohlrausch fit (Eq. 4.1) to the 449-K data, with $f_q^c=0.80$ and $\beta=0.71$. This curve fits the long-time behavior of the experimental data where $\phi_q(t)$ has decayed to ≤0.2 and departures from the von Schweidler decay become significant. The major part of the decay, where $0.9>\phi_q(t)>0.2$, is fully accounted for by the MCT β-decay dynamics.

Within the experimental accuracy of the neutron-scattering experiment, it is possible to fit the data completely with Kohlrausch functions. But since one is then erroneously fitting part of the β-relaxation process along with the α-relaxation process, the f_q^c and β values found from such fits increase with increasing temperature, in apparent violation of the MCT scaling [13,21].

The functions $G(t)$ and $\chi''(\omega)$ contain the same information because they are related by Fourier transformation. However, the equivalence of the information contained in our measurement of the susceptibility over a three-decade-frequency window in Figs. 1(a) and 1(b) on one hand, and the measurement of the decay curves over a three-decade window in time in Fig. 6(a) on the other hand, is hidden. There is no general and direct way to relate the function $\chi''(\omega)$ for a finite internal to the function $G(t)$ for another finite window; nor is there a simple way to map the χ'' data onto the $G(t)$ results. The most significant features of the χ'' data in Figs. 1(a) and 1(b), viz., the minimum for $T>T_c$ and the knee for $T<T_c$, are not easily recognized in the $G(t)$ data in Fig. 6(a). These features can be recovered from $G(t)$, however, if one computes the derivative

$$F(\omega)=\frac{dG(t)}{d(\ln t)},\quad t=2\pi/\omega\ . \tag{4.2}$$

Figure 6(b) shows the results for the $\log_{10}(F)$ versus $\log_{10}(\omega)$ curves calculated for the fit curves from Fig. 6(a). Minima of the curves and a knee in the $T=366$ K curve are clearly visible. So there is equivalence of the information of a susceptibility measurement for the internal $\omega_{\rm min}<\omega<\omega_{\rm max}$ to a measurement of $G(t)$ for the interval $2\pi/\omega_{\rm max}<t\ll2\pi/\omega_{\rm min}$, provided the quantity $F(\omega)$ in (4.2) has the same noise level as $\chi''(\omega)$. In fact, $F(\omega)$ is proportional to $\chi''(\omega)$ if $G(t)$ is a so-called slowly varying function, and this is predicted by MCT in the limit of λ close to unity [5].

B. The Debye-Waller factor

In the first tests of the MCT for CKN, the determination of the Debye-Waller (or nonergodicity) factor f_q played an important role [14]. In the idealized theory, where $f_q=\lim_{t\to\infty}\phi_q(t)$, there will be a jump in f_q as $T\to T_c+$ from 0 to f_q^c followed by a square-root singularity:

$$f_q=\begin{cases}f_q^c+h_q\sqrt{\sigma/(1-\lambda)} & (T<T_c)\\ 0 & (T>T_c)\ .\end{cases} \tag{4.3}$$

In practice, limited experimental resolution results in the measurement of a quasielastic fraction within a narrow energy window rather than the purely elastic fraction f_q. With increasing temperature, the quasielastic fraction does not fall to zero at T_c, but rather to the α-peak area and thus becomes a smoothly varying function of temperature for $T>T_c$ [5]. The finite window may also produce some rounding of the cusp indicated by Eq. (4.3).

In the extended MCT, since $\lim_{t\to\infty}\Phi_q(t)=0$, for all T no such unambiguous definition of f_q is possible. Recently, an effective nonergodicity parameter $\tilde{f}_q$ was defined as the value of $\phi_q(t)$ at the inflection point in $G(t)$ [10]. In the limit $|\sigma|>\sigma_0$ where δt_0 can be neglected, it was found that with this definition

$$\tilde{f}_q=\begin{cases}f_q^c+h_q\sqrt{\sigma/(1-\lambda)} & (T<T_c)\\ f_q^c+h_q\gamma_i\sqrt{|\sigma|} & (T>T_c)\ .\end{cases} \tag{4.4}$$

The solid line in Fig. 7 shows this result for $f_q^c=0.80$ and $h_n(T=T_c)=h$, as found in Fig. 6(a).

For the full β correlator including the temperature-dependent values of σ, h, and δ found from the above analysis, the values $\tilde{f}_q$ were computed numerically and are shown by the points in Fig. 7. The result of the idealized $\delta t_0=0$ theory is seen to be smeared out severely by the effects of the hopping terms. Without knowing $\delta(T)$ and $h(T)$, the form of $\tilde{f}_q(T)$ cannot be predicted and f_q^c cannot be accurately determined. A fit of the data to Eq. (4.3) will always tend to overestimate f_q^c.

Finally, we note that this conclusion is likely to be

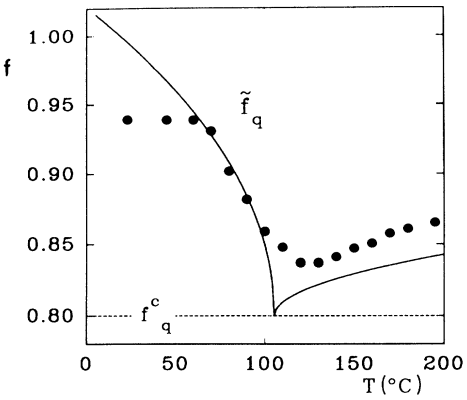

FIG. 7. The effective Debye-Waller factor $\tilde{f}_q$ at q_0 defined by the inflection point t_i of the $G(t)$ vs $\log_{10}(t)$ curves, i.e., $\tilde{f}_q = h_q G(t_i)$. The solid circles are determined from the parameters of Fig. 2 and $f_q^c = 0.80$. The solid lines are the square-root asymptotes of the formula (4.4) law scaled with $h_q(T) = h_q(T_c)$ and the linear fit for $\sigma(T)$ from Fig. 2(a).

highly material dependent. For Salol, where the critical region is much narrower than for CKN, smearing of $f_q(T)$ by hopping effects should be less severe.

V. DETAILS OF EXTENDED MCT ANALYSIS OF SUSCEPTIBILITY SPECTRA

In this section we discuss the influence of activated hopping processes on the susceptibility spectra in more detail and examine some of the subtleties hidden in Fig. 1.

A. CKN

Figure 8 exhibits a scaling plot of $\chi''(\omega)/\chi''_{\min}$ versus $\omega/\omega_{\min}$, obtained by parallel shifts of the data curves from Fig. 1(a), so that the minimum positions coincide. It is the same figure as shown in Ref. [11], but now only

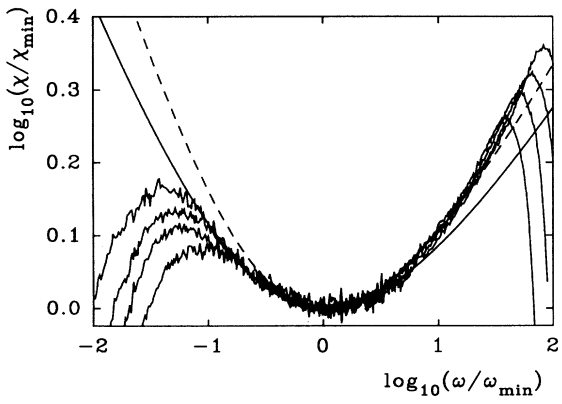

FIG. 8. Scaling plot for CKN according to the idealized theory $\delta=0$ for $T=466$, 453, 443, and 433 K (from bottom to top at the α-peak position.) The solid line is the $\delta=0$ master curve with $\lambda=0.85$ also used in Fig. 1(b). The dashed line is a $\lambda=0.80$ master curve.

those temperatures are included for which δ can be neglected. The full and dashed lines are the master spectra of the idealized MCT for $\lambda=0.85$ and 0.80, respectively. One can see that the fit interval for both choices of λ is about the same. Within the MCT for the ideal liquid to glass transition, i.e., within the simplification of the present theory to $\delta=0$, one finds that for decreasing $(T-T_c)$ the $\hat{\omega}=\omega/\omega_{\min}$ interval, where $\chi''/\chi_{\min}$ is close to the master curve, has to expand. There is a slight trend in this direction on the large $\hat{\omega}$ side for both choices of λ. The effect for small $\hat{\omega}$ is very nicely exhibited for $\lambda=0.85$ but there is no such effect for $\lambda=0.80$. The β regime, by definition, is the one where the scaling holds. There the master function must agree with the data. This is not the case for $\lambda=0.80$. For these reasons we prefer the larger value for the exponent parameter.

Figure 9(a) reproduces from Fig. 1(a) the spectrum for 413 K and its fit with $\delta\neq 0$. The dashed curve and the chain curve are the master functions for $\delta=0$ with $\lambda=0.80$ and 0.85, respectively. Remember that the chain curve is the common shape function identified in Fig. 8 for the $T\geq 433$ K data. One notices that upon lowering T by 20° to 413 K the spectral shape is not changed seriously for $\omega>\omega_{\min}$, but it becomes considerably steeper for $\omega<\omega_{\min}$. This effect is described by the full curve by choosing $\sigma^*=-1.35$. The major effect of the hopping transport in the liquid regime when σ approaches σ_0 is a steepening of the $\log_{10}(\chi'')$ versus $\log_{10}(\omega)$ graph for $\omega<\omega_{\min}$. In describing the high-frequency α peak by an effective power law $\chi''\propto 1/\omega^{\hat{b}}$, $\hat{b}$ would increase with decreasing T. The stochastic hopping dynamics drives the high-frequency α spectrum towards Debye behavior [10]: $\hat{b}\rightarrow 1$. Decreasing λ also steepens the spectral minimum. Indeed the dashed line shows that the ideal theory can account for the data, provided λ is decreased to 0.80. If there was no other information one could not discriminate between the fit possibilities $\lambda=0.85$, $\delta t_0\neq 0$ or $\lambda=0.80$, $\delta t_0=0$. If one searches for an optimal fit for all data with $T\geq 413$ K within the idealized version of the MCT as has been done in Ref. [11], one has to decrease the optimal λ below 0.85.

The aforementioned effects are more pronounced if the separation parameter is decreased even further for $T>T_c$. This is shown in Fig. 9(b) for the data for 393 K. The full curve describes the spectrum well with $\sigma^*=-0.79$; the spectrum is within the transition region. The dashed line is the $\lambda=0.80$, $\delta=0$ master curve. Remember that it describes well the spectrum in Fig. 9(a). Now the data are above the fit curve for $\omega>\omega_{\min}$ as well as for $\omega<\omega_{\min}$. An acceptable fit can be obtained by lowering λ even further. But since this strategy does not work anymore for the next lower value of T, the result is not exhibited as a serious alternative in the figure. A better alternative within the simplified MCT consists of shifting the master curve so that the $\omega>\omega_{\min}$ part of the data is fitted. The chain curve in Fig. 9(b) shows the result. This was the procedure used in Ref. [11]. In this manner one avoids misconclusions concerning the critical exponent a at the expense of placing the theoretical $\omega_{\min}$ somewhat below the experimental one and underestimating the spectrum for $\omega<\omega_{\min}$.

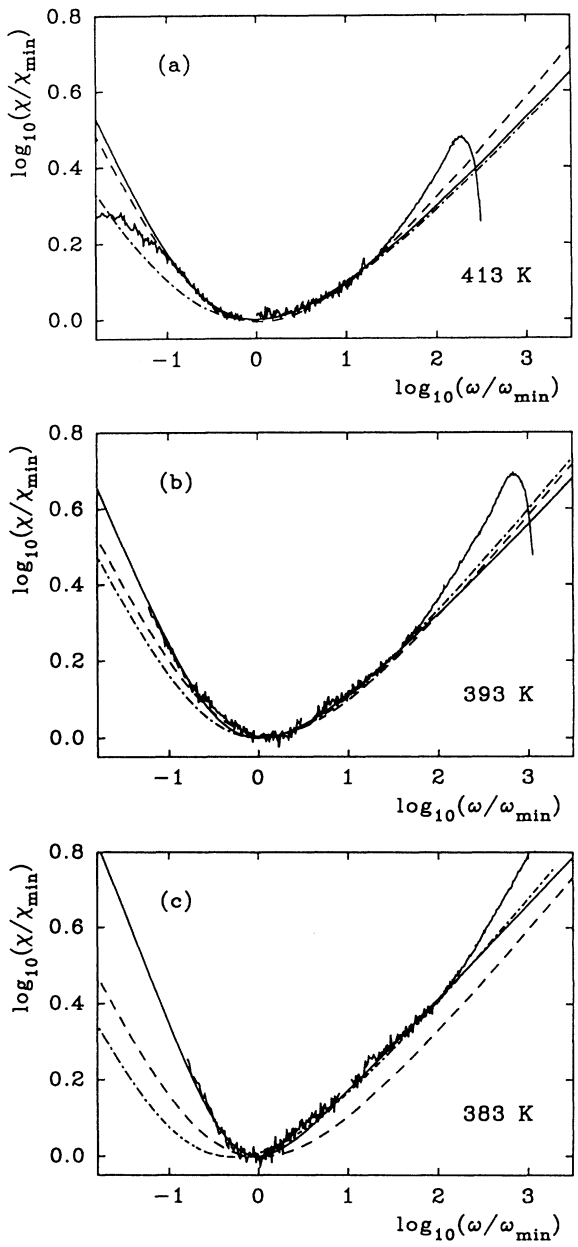

FIG. 9. This figure demonstrates the effects of nonvanishing δ on the CKN data for temperatures above T_c. (a) CKN susceptibility spectrum at $T=413$ K scaled by the minimum position and height. The solid line is the $\lambda=0.85$ fit of Fig. 1(b) where $\sigma/\sigma_0=-1.35$. The dashed and the chain curves are $\delta=0$ master functions for $\lambda=0.80$ and 0.85, respectively. (b) The $T=393$ K spectrum and the fit of Fig. 1(b) (solid line) with $\sigma/\sigma_0=-0.79$. The dashed line shows the master function for $\lambda=0.80$ shifted to coincide with the data at the minimum position whereas the chain curve is the same master function shifted in order to fit the high-frequency wing of the minimum. (c) $T=383$ K spectrum fitted with $\lambda=0.85$ and $\sigma/\sigma_0=-0.047$ (solid line) from Fig. 1(b). The $\lambda=0.80$, $\delta=0$ master curve shifted onto the minimum values is shown as a dashed curve. This master curve is also shown as a chain curve shifted onto the high-frequency wing.

Figure 9(c) reproduces the $T=383$ K data from Fig. 1(a) together with the fit for $\sigma^*=-0.047$, shown as a full curve. It is not possible to fit the spectral minimum by an ω^{-b} to ω^a crossover as predicted by the simplified version of the MCT. Decreasing λ so much that the data for $\omega<\omega_{min}$ are fitted would ruin the fit for $\omega>\omega_{min}$. If the $\lambda=0.80$, $\delta=0$ fit curve, shown as a dashed line, is adapted to the experimental minimum, the data lie above the fit curve for large as well as for small ω. The discrepancies between the $\delta=0$ fit and data would be even greater for the $\lambda=0.85$ curve. The identified phenomenon is the fingerprint for $T\approx T_c$ [10]. For $|\sigma|\ll\sigma_0$ the crossover from the critical spectrum ω^a to the von Schweidler spectrum ω^{-b} (for $\lambda<\lambda_c=\pi/4=0.785$) or $\omega^{-1/2}$ (for $\lambda>\lambda_c$) is rather abrupt. For $\omega>\omega_{min}$ the spectrum exhibits the critical decay rather well, since hopping effects suppress the corrections to the critical spectrum [10]. Here, and only here, one can estimate, as was done in Ref. [22], the exponent a, or the equivalent value for λ, by a simple power-law fit to the data.

In Fig. 10(a) we examine the influence of the temperature dependence of the critical amplitude h and the hopping parameter δt_0 found in Fig. 2 on two commonly used tests of the MCT. In the extended theory including hopping effects the functions $\chi_{min}(\sigma,\delta t_0)$ and $\omega_{min}(\sigma,\delta t_0)$ obey a one-parameter scaling law [10]:

$$\chi_{min}(\sigma,\delta t_0)=\sqrt{\sigma_0}\,h f_2(\sigma/\sigma_0)\ , \tag{5.1a}$$

$$\omega_{min}(\sigma,\delta t_0)t_0=\sigma_0^{1/2a}f_1(\sigma/\sigma_0)\ . \tag{5.1b}$$

Only for $\sigma\ll\sigma_0$ are the known results from the idealized theory obtained: $f_1(x\to-\infty)=\gamma_1^L|x|^{1/2a}$, $f_2(x\to-\infty)=\gamma_2^L|x|^{1/2}$. If δt_0 and h are constants, a plot of $\log_{10}(\chi_{min})$ versus $\log_{10}(\omega_{min})$ yields a straight line for $\sigma\ll-\sigma_0$ (i.e., in the liquid): $\log_{10}(\chi_{min})=\log_{10}(h)+a\log_{10}(\omega_{min}/\omega_0)$. This is demonstrated in Fig. 10(a), where the solid line shows the master function $\chi(\omega_{min})$ on a double logarithmic plot. The values of h and δt_0 at the temperature T_c are used. For $\omega>10$ GHz the master function is a linear law with the mentioned slope a. The point which corresponds to T_c is close to the circle for 383 K. When T_c is approached, deviations from the linear law appear. Lowering the temperature further below T_c, the minimum position starts to increase again. This master function cannot be seen experimentally in general, since h and δt_0 are functions of temperature as shown in Fig. 2. Inserting the fits of $h(T)$ and $\delta t_0(T)$ discussed in context with Fig. 2, the influence on the master function can be tested separately. The changes can be obtained from the master function by inserting the functions $h(T)$ and $\sigma_0(T)$ in Eqs. (5.1).

The dashed curve (long dashes) in Fig. 10(a) is the result of using $h=h(T_c)=$const and the mentioned Arrhenius fit for $\sigma_0(T)$ (see Fig. 2). In the liquid, only small deviations from the master function are observed. In the glass the strong decrease of $\sigma_0(T)$ deforms the master function in a qualitative manner: the position ω_{min} con-

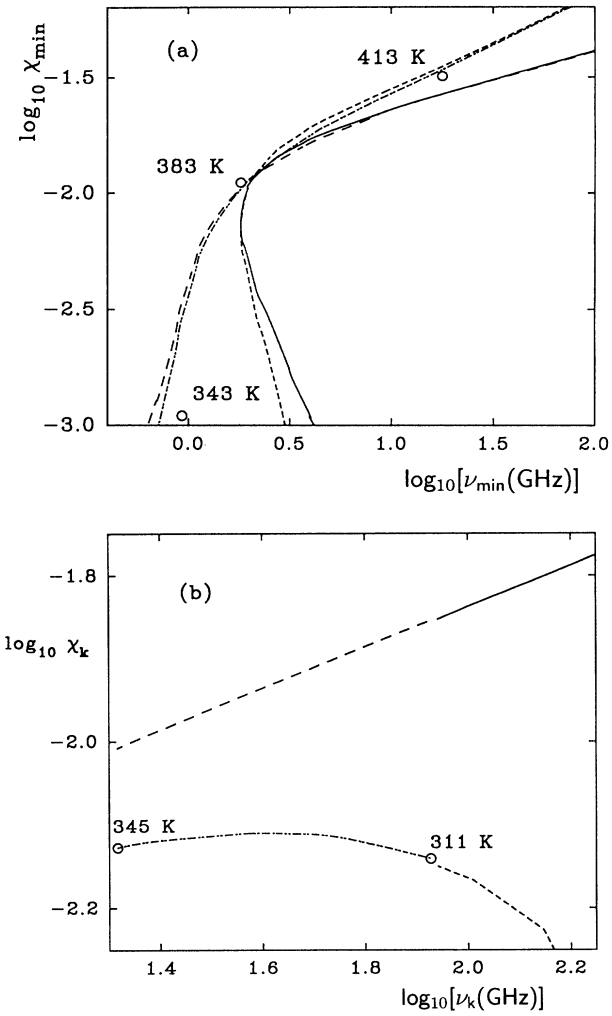

FIG. 10. Cross checks on the minimum and glass knee positions and heights for the CKN analysis. (a) Double logarithmic plot of minimum height vs minimum position for $\lambda=0.85$ with σ values taken from the linear fit of Fig. 2(a). The solid line corresponds to the theoretical scaling curve for constant δ [here $\delta t_0=\delta(T_c)t_0=6.3\times10^{-6}$ and constant $h_{ls}=h_{ls}^c=0.09$]. The long-dashed curve shows the distortion of this scaling curve if δ is varied with temperature in correspondence to the Arrhenius fit of Fig. 2(a); $h_{ls}=h_{ls}^c$ is still kept fixed. The short-dashed curve is obtained if δ is kept fixed at its critical value $\delta=\delta^c$ but h_{ls} varies according to the linear fit of Fig. 2(b). The chain curve results from the scaling curve if $\delta(T)$ and $h_{ls}(T)$ are simultaneously varied with temperature T. (b) Double logarithmic plot of the height vs the position of the glass knee. The curves have the same meaning as in (a). In order for the glass knee to be observable in the theoretical curve σ/σ_0 has to be bigger than a minimal value $\sigma/\sigma_0>4.6$. Depending on the choice for $\delta(T)$ therefore the knee is observable for different σ and consecutively for either $\log_{10}(\omega_k)>1.95$ if $\delta=\delta(T_c)=6.3\times10^{-6}/t_0$ or for $\log_{10}(\omega_k)>1.35$ if δ decreases with decreasing temperature according to the quoted Arrhenius fit. In the first case the knee is observable for $T<311$ K only if σ is varied according to its linear fit; in the experimentally found second case the knee can be seen for $T<345$ K.

tinues to decrease by lowering the temperature instead of increasing. The temperature variation of δt_0 is able to compensate the stiffening of the system. If δt_0 is kept constant [$\delta t_0=\delta t_0(T_c)$] and h varies linearly with temperature (compare to the fit in Fig. 2) the master function is also deformed. The short dashes in Fig. 10(a) show that the slope of $\log_{10}(\chi_{min})$ versus $\log_{10}(\omega_{min})$ is increased in the liquid. This deformation leads to discrepancies between the exponent a obtained by choosing a special λ for the fits to the experimental data and the one obtained by the plot shown in Fig. 10. In the glass the effect of $h(T)$ is small compared to that of $\delta t_0(T)$. $h(T)$ yields only a shift in vertical direction whereas the strong decrease of δt_0 yields a horizontal deformation of the master curve. The chain curve is the experimental result if the temperature dependence of h and δt_0 are included. In the liquid the effect of varying h exceeds the one of $\delta t_0(T)$. Thus the discrepancy between the critical exponent a and the slope of the function $\log_{10}(\chi_{min})$ versus $\log_{10}(\omega_{min})$ in Ref. [11] is explained predominantly by a temperature-dependent critical amplitude h.

If the susceptibility spectrum $\chi''(\omega)$ is divided by $\sqrt{\omega}$ a maximum appears for $\sigma/\sigma_0>4.6$. This maximum corresponds to the crossover from ω^a for high frequencies to ω^1 for low frequencies deep in the glass, i.e., a knee appears in the spectrum. The position ω_k and height χ_k of this knee, where ω_k is the position of the maximum in $\chi''(\omega)/\sqrt{\omega}$ and $\chi_k=\chi(\omega_k)$, obey a one-parameter scaling law [10]:

$$\chi_k(\sigma,\delta t_0)=\sqrt{\sigma_0}\,h f_4(\sigma/\sigma_0)\ , \tag{5.2a}$$

$$\omega_k(\sigma,\delta t_0)=\omega_0\sigma_0^{1/2a}f_3(\sigma/\sigma_0)\ . \tag{5.2b}$$

Since the knee appears only for $\sigma\gg\sigma_0$, the master function $\log(\chi_k)$ versus $\log(\omega_k)$ is the linear law of the idealized theory, $\log_{10}(\chi_k)=\log_{10}(h)+a\log_{10}(\omega_k/\omega_0)$. This is shown by the full curve in Fig. 10(b) with $h=h(T_c)$, $\sigma_0=\sigma_0(T_c)$. With these parameters the knee can be seen only for $T<311$ K. If only the temperature dependence of δt_0 is taken into account, the linear law is not changed since the condition $\sigma/\sigma_0\gg1$ is always fulfilled if the knee can be detected. The result is shown as a long-dashed line in Fig. 10(b). The temperature dependence of δt_0 only causes an upward shift of that temperature at which σ reaches the value $\sigma=4.6\sigma_0$ from 311 to 345 K. It is the decreasing of the critical amplitude that leads to a qualitative deformation of the master function. Assuming $\delta t_0=\delta t_0(T_c)=$const, the fit of h found in Fig. 2 leads to the short-dashed curve in Fig. 10(b). Instead of a monotonously increasing function a decreasing function is obtained. The combination of temperature dependences of h and δt_0 [chain curve in Fig. 10(b)] yields a very flat function. The critical law is completely hidden due to the temperature variation of h. In the tendency these trends can also explain the discrepancy found in Refs. [11,12] between the expected slope (i.e., critical exponent a) of $\log_{10}(\chi_e)$ versus $\log_{10}(\omega_e)$ and the experi-

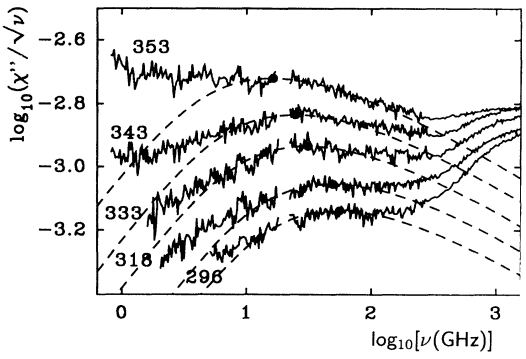

FIG. 11. In a double logarithmic plot of $\chi''(\omega)/\sqrt{\omega}$ vs ω, the glass knee appears as a peak at a position proportional to ω_σ. CKN data for five temperatures, with fits for $\lambda=0.85$, $\delta=0$ are shown. Peak positions are indicated by solid circles. The range of validity of the fits is seen to shrink on the high-frequency side with decreasing temperature.

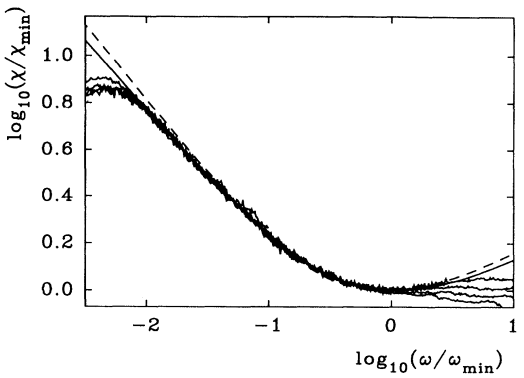

FIG. 12. Scaling plot for Salol according to the idealized $\delta=0$ theory for the temperatures $T=333$, 323, 313, and 303 K from bottom to top at rescaled frequencies larger than 1. The solid line is the $\lambda=0.73$, $\delta=0$ master curve also used in Fig. 1(c). The dashed line is a $\lambda=0.70$ master curve.

mentally observed slope. (The definition of ω_e in Ref. [11] is different than ours, but the qualitative trends due to the temperature variation of h and δt_0 are the same.)

Although the idealized law $\omega_k t_0=\sigma_0^{1/2a} f_3(\sigma/\sigma_0\to\infty)$ $=\sqrt{\sigma}\gamma_3^G$ is not found unambiguously, one of the most challenging predictions of the MCT is the existence of a β-scaling frequency ω_σ, which vanishes in the idealized theory by cooling *and* heating for $T\to T_c$. Especially the phenomenon of slowing down by heating is very uncommon in the physics of glass. The plot of $\chi''(\omega)/\sqrt{\omega}$ versus ω provides an unbiased test of this prediction. Figure 11 shows the result for CKN. If $T\leq 353$ K a peak appears whose position is shifted to higher frequencies if the temperature is lowered. This kind of analysis may even serve as a guide to how the master curves of the idealized theory have to be used for fitting the data below T_c. The dashed curves are master functions for $\delta t_0=0$, $\lambda=0.85$ which attempt to describe the region surrounding the knee.

B. Salol

Figure 12 explains the choice of $\lambda=0.73$ instead of $\lambda=0.70$ for Salol. The data for $T=333$ to 303 K are shifted on a double logarithmic plot until they coincide in the minimum region. The growing of the scaling regime can be seen on the high-frequency side. Contrary to CKN, the β-scaling regime does not change on the low-frequency wing. The von Schweidler law ω^{-b} is very well developed. The β master function for $\lambda=0.73$, $\delta t_0=0$ (solid line) seems to be more adequate to describe this feature than the master function $\lambda=0.70$, $\delta t_0=0$ (dashed line).

Lowering the temperature down to 263 K, the fit with the idealized theory $\lambda=0.70$, $\delta t_0=0$ remains a remarkably good fit as shown in Fig. 1(c). $\lambda=0.73$ can only be used if activated hopping processes are included. The fit with $\lambda=0.73$, $\delta t_0=0$ exhibits the same deficiencies as, e.g., explained in Fig. 9(a) for CKN, $\lambda=0.85$ and $\delta t_0=0$. Figure 13(a) shows that there is no difference at all in the quality of the fits with $\delta t_0=0$, $\lambda=0.70$ and $\delta t_0\neq 0$, $\lambda=0.73$. But Fig. 13(b) demonstrates that for $T=253$ K, no fit with $\lambda=0.70$, $\delta t_0=0$ is possible. The same signature is found as for CKN at $T=383$ K [Fig. 5(c)]. Only the high-frequency wing can reasonably be described by $\lambda=0.70$, $\delta t_0=0$. Choosing $\lambda=0.73$ and $\sigma/\sigma_0=-0.411$ a good fit of the whole minimum region is obtained; com-

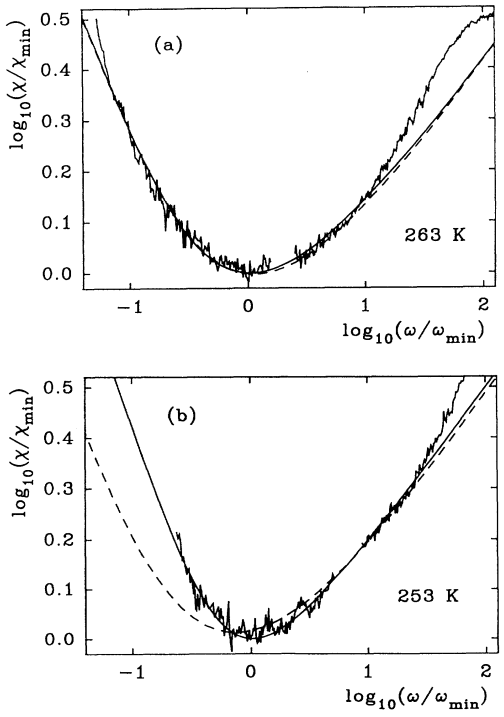

FIG. 13. This figure exemplifies the effects of $\delta\neq 0$ in the Salol data above T_c at (a) $T=263$ K and (b) $T=253$ K. The β fits taken from Fig. 1(c) correspond to $\lambda=0.73$, with $\sigma/\sigma_0=-2.43$ and -0.411, respectively. Dashed curves indicate $\lambda=0.70$, $\delta=0$ fits.

pared to $T=263$ K [Fig. 13(a)], σ/σ_0 is changed by a factor 6. This dramatic change within 10 K from $|\sigma/\sigma_0|>1$ to $|\sigma/\sigma_0|<1$ explains why in Fig. 13 the idealized theory can correctly describe the data for $T\geq 263$ K but completely fails for $T=253$ K.

The crossover temperature T_c lies between 243 and 253 K, since the data at $T=243$ K can only be explained by a master curve with $\sigma>0$ as shown in Fig. 14. The value $\sigma/\sigma_0=1.86$ is not big enough that the ω^1 asymptote of the idealized theory could be reached for low frequencies. The knee which can be seen in the fit $\delta t_0=0$, $\lambda=0.70$ as well as in the fit $\delta t_0\neq 0$, $\lambda=0.73$ (Fig. 14) is not visible in the data since the corrections to the asymptotic result due to the microscopic peaks are too big. For the lowest temperature $T=198$ K (Fig. 1), $\sigma/\sigma_0=18.8$ has to be chosen. For this value the ω^1 asymptote seems to be reached for low frequencies, but the knee is still hidden by corrections to the asymptotic form.

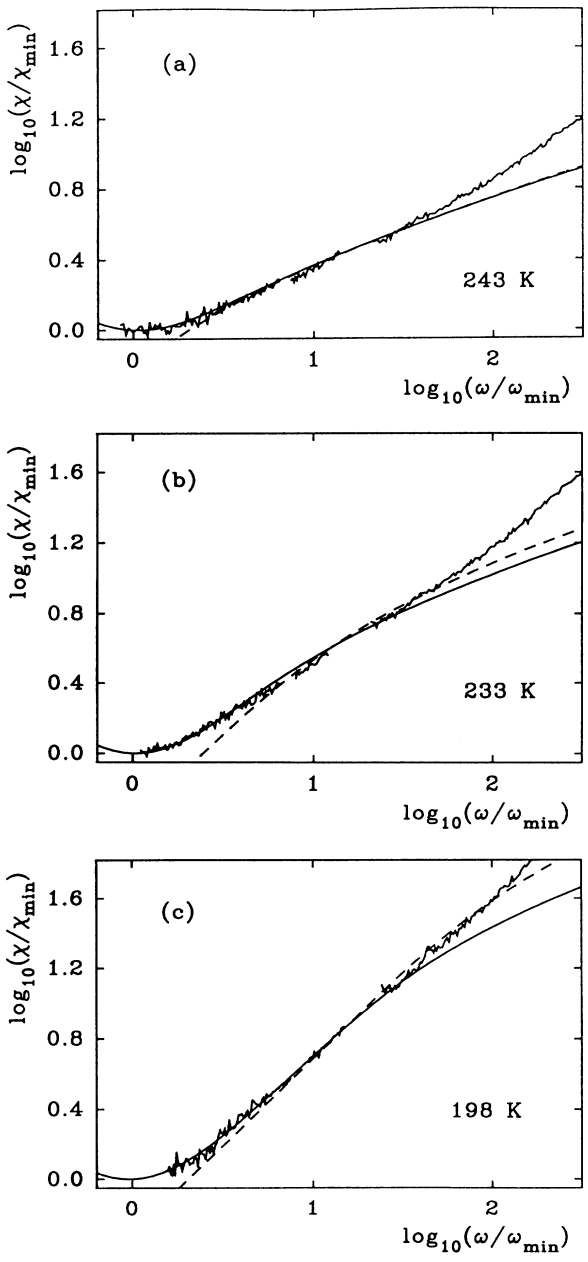

FIG. 14. The characteristic effect of $\delta\neq 0$ on glass curves $T<T_c$ for Salol. For the three temperatures (a) $T=243$ K, (b) $T=233$ K, and (c) $T=198$ K the data, the corresponding fits of Fig. 1(c) (solid lines), and an optimized fit with $\lambda=0.70$, $\delta=0$ (dashed line) are shown. The parameters $\sigma/\sigma_0=1.86$, 5.05, and 18 are chosen for (a), (b), and (c), respectively.

VI. SUMMARY AND CONCLUSIONS

The susceptibility spectra $\chi''(\omega)$ of CKN and Salol, determined from depolarized-light-scattering experiments [11,12], have been reanalyzed using the extended MCT β-correlation functions which are solutions of Eq. (2.16). The analysis has revealed the trajectories C followed in the $(\sigma,\delta t_0)$ plane as the temperature is lowered from the liquid region throughout the transition region, and into the region of glassy dynamics. The transition region, where relaxation dynamics are dominated by the δt_0 hopping terms, extends over ~ 40 K in CKN and is considerably narrower in Salol.

The theoretically computed susceptibility spectra provide significantly better fits to the experimental data than the originally published theoretical spectra which were computed using the idealized version of MCT with hopping terms neglected, i.e., with $\delta t_0=0$. Furthermore, the current theoretical spectra provide specific predictions for the positions of the susceptibility minima at temperatures below T_c which should be accessible to experimental measurement.

We have also shown that the correlation functions found from the current fits can explain the CKN neutron spin-echo data of Mezei *et al.*, eliminating the apparent disagreement with the scaling prediction of MCT which resulted from neglect of the contribution of the β-relaxation process [13]. We found that almost all of the neutron data follow the β-relaxation dynamics, except at the longest times for the highest temperatures where a crossover from power-law to stretched-exponential (Kohlrausch) behavior occurs. An important aspect of this agreement which we emphasize is that within the precision of the experiments the β-correlation functions for the light-scattering and neutron-scattering experiments are equivalent, as required by MCT.

We note that the extended MCT, used here to analyze experimental data quantitatively for the first time, eliminates the obviously nonphysical predictions of the idealized MCT such as the complete arrest of the α-relaxation process at T_c and the disappearance of the susceptibility minimum below T_c. Similarly, as discussed by Sjögren [9], the extended MCT also eliminates the unphysical viscosity divergence at T_c, predicting instead a crossover from an algebraically diverging T dependence to Arrhenius dependence.

The solutions of the MCT equations of motion are not known for conventional glass-forming liquids. However, the qualitative features of the solutions can be inferred from the known asymptotic laws valid for parameters

close to the glass-transition singularity. By performing a quantitative comparison of the asymptotic laws with data, one can determine to what extent MCT is able to explain the qualitative features of supercooled-liquid dynamics. From the analysis reported here we conclude that the theory can successfully explain the presently known experimental facts for the β relaxation of CKN and Salol. Some specifications and reservations shall be added.

The asymptotic laws of MCT do not include corrections to scaling. The properties of these corrections are now known. They may be larger in one system than in another, and will depend on the variable X under discussion. We found that the corrections are small within a three decade dynamical window for CKN for light scattering and for neutron-scattering data for a certain wave vector q. It is quite possible that for neutron-scattering data for a different wave vector the range of applicability of Eq. (2.6) is not so surprisingly large as demonstrated in Fig. 6.

Figure 1 shows that the β-relaxation formulas account for the major part of the high-frequency wing of the α peak. This holds for CKN for $T > 393$ K and Salol for $T > 273$ K. Within the MCT for the β process, the α peak itself also appears as a correction to the scaling law. From numerical solutions for so-called schematic models for the MCT one knows that indeed occasionally the von Schweidler asymptote accounts for a major part of the α spectrum. But one knows also that in other cases the von Schweidler law describes only the uppermost part of the α peak [19]. So it appears more as an accident that our formulas work so well on such large dynamical ranges as shown in Figs. 1 and 6. One should not be surprised if the implication of Eq. (2.6) with our $G(t)$ or $\chi''(\omega)$ for other measurements like neutron scattering for other wave vectors or dielectric loss spectra do not work for such large $\log_{10}(t)$ or $\log_{10}(\omega)$ intervals as we found in this paper.

The center of the β spectrum, i.e., the susceptibility minimum, depends most sensitively on the two relevant control parameters σ and δ. If our measurement could be extended to lower frequencies so that the susceptibility minimum falls within the accessible dynamical window also for $T < T_c$, the uncertainties for the fitting parameters σ and δ could be reduced considerably. Thereby the uncertainties of other parameters like λ could be reduced as well.

A drastic correction to the scaling law results is obvious if one compares the spectra for CKN with those for Salol. The critical power-law form is so well developed for CKN that one can read off the proper exponent $a \sim 0.3$ from raw data for 373 K in Fig. 1(a). Similarly, one notices the knee in the spectra for $T \lesssim 343$ K and the decrease of the frequency ω_e for the knee position with increase of T, particularly if one plots the data as $\chi''(\omega)/\sqrt{\omega}$ versus $\log_{10}(\omega)$ as shown in Fig. 11. The existence of the knee is the predicted fingerprint for the $T < T_c$ states. The softening of the dynamics upon heating, exhibited by the ω_e versus T curves, is a predicted melting precursor for the arrested glass structure. Neither of the mentioned features can be inferred directly from the raw data for Salol. Crystalline Salol has an excitation band near 400 GHz [12]. It leads to a low-lying excitation band for the liquid, which is unrelated to those structural relaxation phenomena we want to study. It appears as a correction to the leading-order scaling results, which masks completely the specified two glass-transition phenomena.

ACKNOWLEDGMENTS

We thank F. Mezei for providing the CKN neutron spin-echo data discussed in Sec. IV and L. Sjögren for helpful comments on the manuscript. Research at CCNY was supported by the U.S. National Science Foundation under Grant No. DMR-9014344.

*Also at Max-Planck-Institut für Physik (Werner Heisenberg Institut), D8000 Müchen, Germany.
†Present address: Institute for Physical Science, University of Maryland, College Park, MD 20742.
‡Present address: Dept. of Physics, Florida International University, Miami, FL 33199.

[1] J. Wong and C. A. Angell, *Glass Structure by Spectroscopy* (Dekker, New York, 1976).
[2] G. W. Scherer, *Relaxation in Glasses and Composites* (Wiley, New York, 1986).
[3] E. Leutheusser, Phys. Rev. A **29**, 2765 (1984).
[4] U. Bengtzelius, W. Götze, and A. Sjölander, J. Phys. C **17**, 5915 (1984).
[5] For extensive reviews, see W. Götze and L. Sjögren, Rep. Prog. Phys. **55**, 241 (1992); W. Götze, in *Liquids, Freezing and the Glass Transition,* edited by J. P. Hansen, D. Levesque, and J. Zinn-Justin (North-Holland, Amsterdam, 1992), p. 287.
[6] S. P. Das and G. F. Mazenko, Phys. Rev. A **34**, 2265 (1986).
[7] W. Götze and L. Sjögren, Z. Phys. B **65**, 415 (1987).
[8] W. Götze and L. Sjögren, J. Phys. C **21**, 3407 (1988).
[9] L. Sjögren, Z. Phys. B **79**, 5 (1990).
[10] M. Fuchs, W. Götze, S. Hildebrand, and A. Latz, J. Phys. Condens. Matter **4**, 7709 (1992).
[11] G. Li, W. M. Du, X. K. Chen, H. Z. Cummins, and N. J. Tao, Phys. Rev. A **45**, 3867 (1992).
[12] G. Li, W. M. Du, A. Sakai, and H. Z. Cummins, Phys. Rev. A **46**, 3343 (1992).
[13] F. Mezei, Ber. Bunsenges. Phys. Chem. **95**, 1118 (1991); J. Non-Cryst. Solids **131-133**, 317 (1991).
[14] F. Mezei, W. Knaak, and B. Farago, Phys. Rev. Lett. **58**, 571 (1987); Phys. Scr. **T19**, 363 (1987).
[15] S. F. Edwards and P. W. Anderson, J. Phys. F **5**, 965 (1975).
[16] N. J. Tao, G. Li, X. Chen, W. M. Du, and H. Z. Cummins, Phys. Rev. A **44**, 6665 (1991).
[17] W. Götze, J. Phys. Condens. Matter **2**, 8485 (1990).

[18] W. Götze and L. Sjögren, J. Phys. C **20**, 879 (1987).
[19] M. Fuchs, W. Götze, I. Hofacker, and A. Latz, J. Phys. Condens. Matter **3**, 5047 (1991).
[20] W. Knaak, F. Mezei, and B. Farago, Europhys. Lett. **7**, 529 (1988).
[21] M. Fuchs, W. Götze, S. Hildebrand, and A. Latz, Z. Phys. B **87**, 43 (1992).
[22] N. J. Tao, G. Li, and H. Z. Cummins, Phys. Rev. Lett. **66**, 1334 (1991).